Resonance Properties of Optical All-Dielectric Metamaterials Using Two-Dimensional Multipole Expansion

Efthymios Kallos and Ioannis Chremmos and Vassilios Yannopapas

Resonance Properties of Optical All-Dielectric Metamaterials Using Two-Dimensional Multipole Expansion

Efthymios Kallos[1], Ioannis Chremmos[2], Vassilios Yannopapas[1]

[1]Department of Materials Science, University of Patras, GR-26504, Patras, Greece

[2]Department of Applied Mathematics, University of Crete, GR-71003, Heraklion, Greece

We examine the electromagnetic response of metamaterial unit elements consisting of dielectric rods embedded in a non-magnetic background medium. We establish a theoretical framework where the response is described through the electric and magnetic multipole moments that are simultaneously generated via the polarization currents that are excited upon the incidence of plane waves. The corresponding dipole and quadrupole polarizabilities are then calculated as a function of the Mie scattering coefficients, and their resonances are mapped for the case of dielectric cylindrical rods as a function of the geometry and the material parameters utilized. The results provide critical insight on the anisotropic response of two-dimensional rod-type metamaterials and can be used as a unified methodology in the calculation of exotic effective electromagnetic parameters involved in phenomena such as optical magnetism.

PACS numbers: 42.25.Fx, 78.67.Pt, 78.67.Qa

I. INTRODUCTION

The scaling of metamaterials down to optical and visible frequencies is currently one of the most exciting efforts in the field of artificial materials,[1, 2] allowing the realization of structures with exotic electromagnetic properties which are unachievable using conventional materials. Potential applications in this new frontier of science include subwavelength imaging,[3] cloaking,[4-6] biosensing,[7] and solar power harvesting[8-10]. However, the miniaturization process towards this frequency regime has not been straightforward as the metamaterials designed for microwave frequencies cannot be simply scaled down to operate at optical frequencies without significant losses arising, especially when artificial magnetism is considered. One of the main causes of this situation is the fact that while negative permittivity can be readily available in the optical range using plasmonic materials,[11] natural optical magnetism disappears at high frequencies[12] and artificially generated conduction currents cannot extend beyond THz frequencies[13]. Furthermore, the inclusion of metallic components in optical metamaterials is usually associated with unwanted losses and saturation effects inherent to metals[14].

In order to overcome these issues, the idea of constructing periodic composite media only from non-metallic, dielectric components is being actively explored[15-17]. Similar to metallic metamaterials, the goal is to resonantly generate exotic permittivity and permeability properties in a tunable fashion over a certain frequency range. Unlike metallic metamaterials, the physical mechanism involved here is the resonant excitation of fields via the polarization currents of the bound electrons in the dielectric materials that flow under external illumination. Once these polarization currents are excited they can be considered as a source, giving rise to corresponding local fields, which in turn determine the macroscopic artificial electromagnetic properties of the material. Exotic effective permittivity and permeability values are expected around the frequency regions where the dielectric unit elements under illumination naturally resonate. For a given incident illumination, these regions depend on the shape, size, and permittivity of the dielectric resonator, as well as on the periodic pattern of the composite structure.

This mechanism has been experimentally examined in the literature mostly at microwave frequencies (6 – 10 GHz), where left-handed structures have been fabricated[18-21] using high-ε materials such as barium strontium titanate (BST, with relative permittivity ε~600). Negative permeability has also been demonstrated by Ginn *et al.* in the mid-infrared (43 THz) fabricating a square lattice of Tellurium (ε~25) cubes[22], while Limberopoulos *et al.* fabricated an isotropic negative index metamaterial in the visible range (632 nm) using silicon carbide (ε~7) spheres embedded in a magnesium diboride (MgB_2) plasmonic host[23]. In other numerical analyses aimed at left-handed behavior at optical frequencies, negative permeability is typically achieved using one type of dielectric spheres, while negative permittivity is simultaneously achieved using a second type of spheres,[24, 25] coated spheres,[26] and/or a plasmonic[27, 28] or polaritonic[29] material such as MgB_2 or $LiTaO_3$.

In this paper, instead of focusing on isotropic dielectric metamaterials, we are interested in metamaterials consisting of dielectric rods which could have, as an example, square or circular cross sections. These structures extend much longer along one spatial dimension, and can be effectively treated as two dimensional. While the isotropy provided by several 3D metamaterials is desirable for certain applications, such 2D structures have inherently anisotropic properties which can be in principle tuned independently, thus realizing the primary purpose of metamaterials, which is to provide artificial electromagnetic properties along different directions in space. For example, many of the exciting devices envisioned through transformation optics require anisotropic material parameters,[30] which are not easy to obtain using inherently isotropic structures such as spheres, especially in the optical regime.

Research on rod-type dielectric metamaterials has also been investigated in the literature. O'Brien and Pendry in 2002 first suggested the possibility of generating negative permeability at 4 GHz using a square lattice of BST cylinders[31]. Peng *et al*. in 2007 then experimentally showed negative index behavior at 6.8 GHz using random arrays of square rods,[18] which seems to be the only conclusive demonstration of

left-handedness using dielectric rods at any frequency. A few theoretical designs aimed at harnessing magnetic resonances in dielectric rod metamaterials have emerged since, including concepts at GHz frequencies using BST[32, 33] or ferrites,[34] at 25 THz using silicon carbide[35], and at visible frequencies assuming hybrid silver-semiconductor rods[36]. Most notably, Vynck *et al*. theoretically showed in 2009 that the magnetic resonances could occur down to optical wavelengths (1.55 μm) using lattices of silicon (ε~12) rods,[37] by expanding the fields into a series of multipole excitations. Other materials with high permittivity values in the visible range that could be utilized are Germanium, aluminum arsenide and aluminum antimonide.

It was recently demonstrated experimentally by Evlyukhin *et al*. that silicon structures do indeed support such multipole resonances at visible frequencies, at least for the case of spherical nanoparticles[38]. This implies that, by controlling the multipole resonances in high-ε dielectric rods, effective medium metamaterials could be available in the very near future for the visible regime. The successful fabrication of polaritonic rod arrays for THz frequencies[39] provides positive evidence in that direction as well. However, a universal theoretical modeling of such rod-type dielectric resonators is not available in the literature, especially when the multipole approach is considered. This is the goal of this paper.

The idea behind the multipole expansion is the following: when an electromagnetic wave is incident upon a dielectric particle and therefore polarization currents are excited inside its volume, the currents and the particle can be replaced by multipoles of various orders (dipole, quadrupole, etc.) that act as equivalent point sources for the scattered fields (in the case of long rods, multipoles per unit length are considered). In this paper we establish a theoretical framework that explores this idea for non-magnetic rods, such as cylinders made from dielectric, plasmonic, or conductive materials. The great advantage of this multipole approach is that its results can be directly fed into effective medium models that predict the electromagnetic parameters of composite media[40, 41], since such models typically utilize the electric and magnetic polarizabilities of the array unit elements.

The multipole expansion in two dimensions is quite different and, in fact, more complicated compared to the usual three dimensional expansion readily available[42-44], due to the anisotropic nature of the rod geometry. Our framework utilizes the 2D Green's function, is valid for both polarizations and includes multipole excitations up to the electric quadrupole term. In addition to the field expressions everywhere in space, we also derive the electric and magnetic polarizabilities of 2D rods for all axes as a function of the Mie scattering coefficients. Furthermore, we also identify the locations of the polarizability resonances for the case of cylindrical rods as a function of the rod's normalized radius, their permittivity, and the host material (which can be a plasmonic material). The resonant behavior under the quasistatic and static approximation is also examined. The results provide a fresh, rigorous framework in describing dielectric metamaterials, which is particularly useful when calculating their electromagnetic

response. Note that for the sake of clarity we only examine resonances arising from single rods in this work; the effect of considering the rods in arrays will be explored in a subsequent publication.

II. ELEMENTS OF 2D MULTIPOLE THEORY

In this section we describe the main principles of multipole theory, and highlight the differences between the 2D and the 3D treatment. The 2D scenario assuming a cylindrical coordinate system implies that $\partial/\partial z = 0$ for all quantities involved. We start by assuming an electric current distribution $\vec{J}(\vec{r}')$ in a region of space described through the position vector $\vec{r}'$ which acts as a source for the excited fields $\vec{E}(\vec{r}')$ and $\vec{H}(\vec{r})$ everywhere in space, described through the position vector $\vec{r}$. See Figure 1 for a schematic of the system for the case of a dielectric cylindrical rod. In this case $\vec{J}$ is the polarization current, which vanishes outside the cylinder. A harmonic time dependence $e^{-j\omega t}$ is assumed.

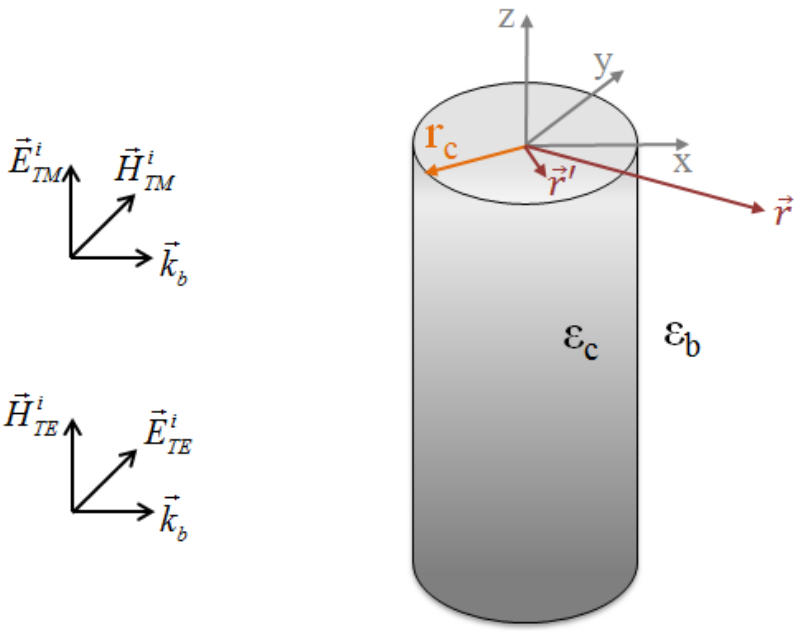

Figure 1: Schematic setup of the dielectric rod system under examination. The cylinder has a radius r_c and relative permittivity ε_c, embedded in a background medium with relative permittivity ε_b. The system is illuminated by perpendicularly incident TE and TM plane waves, exciting polarization currents along the rod. $\vec{r}'$ spans the volume of the rod where the polarization source currents are nonzero, while $\vec{r}$ denotes an observation point.

In the multipole theory, the excited fields are expanded as a summation series of multipole moments, i.e. integrals of quantities that have the form $J \cdot r^n$, where n is a positive integer. For example, the first moments (per unit length) that occur for $n = 0,1$ are the electric dipole moment $\vec{p}$, the magnetic dipole moment $\vec{m}$, and the electric quadrupole moment $\ddot{Q}$, defined as

$$\begin{aligned} \vec{p} &= \frac{j}{\omega}\int_S \vec{J}(\vec{r}')\,dS' \\ \vec{m} &= \frac{1}{2}\int_S \vec{r}' \times \vec{J}(\vec{r}')\,dS' \\ \ddot{Q} &= \frac{j}{\omega}\int_S \left[\vec{J}\otimes\vec{r}' + \vec{r}'\otimes\vec{J}\right] dS' \end{aligned} \quad , \tag{1}$$

where $\vec{a}\otimes\vec{b} = \vec{a}\vec{b}$ is the dyadic product of two vectors. The integration takes place on the 2D surface where the current is non-zero. Then the generated fields can be approximately written as[45]

$$\begin{aligned} \vec{E}/Z_b &\simeq \left[k_b^2 \vec{p} c_b G + (\vec{p} c_b \cdot \nabla)\nabla G\right] + jk_b\left[\nabla G \times \vec{m}\right] - \frac{1}{2}\left[k_b\left(\omega\ddot{Q}\cdot\nabla G\right) + \frac{1}{k_b}\nabla\left(\omega\ddot{Q} : \nabla\nabla G\right)\right] \\ \vec{H} &\simeq -jk_b\left[\nabla G \times \vec{p} c_b\right] + \left[k_b^2 \vec{m} G + (\vec{m}\cdot\nabla)\nabla G\right] + \frac{j}{2}\left[\nabla \times \left(\omega\ddot{Q}\cdot\nabla G\right)\right] \end{aligned}, \tag{2}$$

where k_b, c_b, Z_b are the wavevector, speed of light, and wave impedance in the background medium, respectively, $\nabla = \hat{n}\frac{\partial}{\partial r}$ ($\hat{n}$ is a cylindrical unit vector along the radial direction), and the dependence on $\vec{r}$ has been suppressed for brevity. $\ddot{A} : \ddot{B}$ defines the double-dot product of the dyadics $\ddot{A}$ and $\ddot{B}$. Expression (2) is valid for both 2D and 3D scenarios, with the difference that in 2D the scalar cylindrical Green's function is utilized: $G = \frac{j}{4}H_0^{(1)}(k_b r)$, where $H_0^{(1)}$ is the Hankel function of the first kind and order zero. Note that these moments are derived by expanding the Green's function $G(\vec{r} - \vec{r}')$ around $\vec{r}'$, and so higher order moments are ignored since in general they become increasingly weaker as long as $k_b r' \ll 1$. The detailed procedure for obtaining this multipole field description is outlined in the Appendix.

There are three main reasons why this type of description for the fields using multipole moments is advantageous, especially for metamaterials. First, the fields depend linearly on the moments without involving complicated integrals or geometric and material characteristics of the metamaterial unit element – all this information is replaced by the point-like definition of the moments, offering a useful layer of abstraction in the description. The moments can be assumed known, extracted either via analytical methods (for example for cylinders) or via numerical simulations. Second, many homogenization effective medium theories such as the Maxwell-Garnett[40] or other nonlocal approaches[41] directly utilize the dipole polarizabilities of the unit elements in their description as well. These are directly related to dipole moments and we would like our formalism to be consistent with these methodologies. Finally,

there is a crucial physical link between the multipole moments and the well-known Mie scattering coefficients,[46] at least for the case of cylindrical rods: multipole terms of a given order n have approximately the same dependence on distance as the Mie coefficients do, $\sim(r/r_c)^n$, r_c being the cylinder diameter[47]. Thus, from a physics perspective, we would expect to express the unknown multipole moments as a function of the Mie coefficients of a unit element.

The main difference between the 2D and the 3D multipole expansion method lies in the description of the electric quadrupole moment defined in Eq. (1). Written explicitly, and since $\partial/\partial z = 0$, we get

$$\ddot{Q} = \frac{j}{\omega}\int_S \begin{pmatrix} 2x'J_x & x'J_y + y'J_x & x'J_z \\ x'J_y + y'J_x & 2y'J_y & y'J_z \\ x'J_z & y'J_z & 0 \end{pmatrix} dS' = \begin{pmatrix} Q_{xx} & Q_{xy} & -2\frac{j}{\omega}m_y \\ Q_{xy} & Q_{yy} & 2\frac{j}{\omega}m_x \\ -2\frac{j}{\omega}m_y & 2\frac{j}{\omega}m_x & 0 \end{pmatrix}, \tag{3}$$

where the indices specify the vector component along a particular spatial direction. We observe that in this 2D case the longitudinal current along the z-direction, J_z, decouples from the transverse currents J_x and J_y. As a result only four nonzero electric quadrupole terms appear, while the other terms degenerate into magnetic dipole moments m_x and m_y. Thus, depending on what currents are excited, the behavior of the system is significantly different. If the unit element is excited by a TM wave ($\vec{E} \parallel \hat{z}$), J_z currents only will be generated and the electric quadrupole terms in Eq. (3) vanish. On the other hand, if the excitation is a TE wave ($\vec{E} \perp \hat{z}$), transverse currents will be excited and only the four pure quadrupole terms in Eq. (3) are nonzero. In this case, and since the current flows normal to the surface of the rod, the quadrupole moments are second-order moments of both the volume and the surface polarization charges that developed in the cylinder (see the Appendix for details). It should be noted that the degenerate magnetic dipole terms m_x, m_y that appear in the quadrupole matrix in Eq. (3) contribute to the fields (Eq. (2)) in addition to the pure magnetic dipole terms.

Keeping these considerations in mind, after some algebraic manipulations Eq. (2) can be rewritten in cylindrical coordinates as follows for TM and TE waves everywhere in space:

$$
\begin{aligned}
\vec{E}_{TM} / Z_b &= +k_b^2 \hat{z}\left[p_z c_b G + 2 m_\varphi j G' \right] \\
\vec{H}_{TM} &= +2k_b^2 \left[\hat{n} m_n \left(G + G'' \right) + \hat{\varphi} m_\varphi \left(G + \frac{G'}{k_b r} \right) \right] + k_b^2 \hat{\varphi}\left[p_z c_b j G' \right]
\end{aligned}
$$

$$
\begin{aligned}
\vec{E}_{TE} / Z_b &= +k_b^2 \left[\hat{n} p_n c_b \left(G + G'' \right) + \hat{\varphi} p_\varphi c_b \left(G + \frac{G'}{k_b r} \right) \right] - k_b^2 \hat{\varphi}\left[m_z j G' \right] \\
&\quad - \frac{k_b^2}{2} \left[\hat{n} \omega Q_{nn} \left(G' + G''' \right) + \hat{n} \omega Q_{\varphi\varphi} \left(\frac{G''}{k_b r} - \frac{G'}{\left(k_b r \right)^2} \right) + \hat{\varphi} \omega Q_{n\varphi} \left(G' - \frac{2G'}{\left(k_b r \right)^2} + \frac{2G''}{k_b r} \right) \right] \\
\vec{H}_{TE} &= -k_b^2 \hat{z} \left[p_\varphi c_b j G' - m_z G - \frac{j}{2} \omega Q_{n\varphi} \left(G'' - \frac{G'}{k_b r} \right) \right]
\end{aligned}
\qquad . \qquad (4)
$$

Here the primes denote derivatives with respect to the argument $k_b r$ when applied to the Green's function, while $Q_{nn} = Q_{xx} \cos^2 \varphi + Q_{xy} \sin 2\varphi + Q_{yy} \sin^2 \varphi$, $Q_{\varphi\varphi} = Q_{xx} \sin^2 \varphi - Q_{xy} \sin 2\varphi + Q_{yy} \cos^2 \varphi$, and $Q_{n\varphi} = Q_{xy} \cos 2\varphi + \frac{1}{2}\left(Q_{yy} - Q_{xx} \right) \sin 2\varphi$. Note that Q_{nn} and $Q_{n\varphi}$ are also the components of the vector $\ddot{Q} \cdot \hat{n}$ along the $\hat{n}$ and $\hat{\varphi}$ directions, respectively. We also define that $p_n = p_x \cos\varphi + p_y \sin\varphi$ and $p_\varphi = p_y \cos\varphi - p_x \sin\varphi$, and similarly for m_n, m_φ. Note that the quantities $p_n, p_\varphi, m_n, m_\varphi$ are the projections of the moments along the corresponding directions, and should not be confused with radial and azimuthal components since the dipoles $\vec{p}, \vec{m}$ are located at the origin of the axes.

Some physical insight can be gained for the above field expressions if they are written in their approximate forms for the far and near fields. In the far field ($k_b r \gg 1$), the total fields become

$$
\begin{aligned}
\vec{E} / Z_b &\overset{k_b r \gg 1}{\simeq} +k_b^2 \left[+\hat{\varphi} \left(p_\varphi c_b + m_z - \frac{j}{2} \omega Q_{n\varphi} \right) + \hat{z} \left(p_z c_b - 2 m_\varphi \right) \right] G_\infty \\
\vec{H} &\overset{k_b r \gg 1}{\simeq} +k_b^2 \left[+\hat{z} \left(p_\varphi c_b + m_z - \frac{j}{2} \omega Q_{n\varphi} \right) - \hat{\varphi} \left(p_z c_b - 2 m_\varphi \right) \right] G_\infty
\end{aligned}
\qquad . \qquad (5)
$$

with $G_\infty = \frac{j}{4}\sqrt{\frac{2}{\pi k_b r}}e^{+j(k_b r-\pi/4)}$ being the far-field approximation of the Green's function. The fields behave as typical TEM radiation fields in this case, satisfying $\vec{H} = \hat{n}\times E/Z_b$. The factor of 2 that appears in front of the magnetic moment m_φ originates from the quadrupole moment degeneration in the TM case described earlier in this section. In the near field ($k_b r \ll 1$), the total fields become (retaining only the strongest terms)

$$\begin{aligned} \vec{E}/Z_b &\overset{k_b r\ll 1}{\simeq} +\frac{\hat{n}p_n c_b - \hat{\varphi}p_\varphi c_b}{2\pi r^2} + \frac{1}{k_b}\frac{\hat{n}\left(\omega Q_{nn} - \omega Q_{\varphi\varphi}\right) - \hat{\varphi}2\omega Q_{n\varphi}}{2\pi r^3} \\ \vec{H} &\overset{k_b r\ll 1}{\simeq} +\frac{\hat{n}m_n - \hat{\varphi}m_\varphi}{\pi r^2} + j\frac{\hat{z}\omega Q_{n\varphi}}{2\pi r^2} \end{aligned} \tag{6}$$

There are two ways how Eqs. (4)-(6) can be utilized. One can start with an electric current distribution $\vec{J}$, calculate the multipole moments using Eq. (1), and then evaluate the fields from Eqs. (4)-(6). Alternatively, a single multipole moment can be considered as a source and be inserted directly into Eqs. (4)-(6) for the evaluation of the fields. For example, two parallel, z-oriented uniformly and opposite charged lines separated by a small distance are equivalent to an electric dipole moment per unit length, such as $\vec{p} = \hat{x}p_x$. When plugged into Eq. (6), the static electric field of this system is correctly obtained.

Figure 2 presents a graphical representation of the multipole fields excited for an incident monochromatic TM wave (with free space wavelength $\lambda_0 = 632nm$) propagating along the x (horizontal) direction onto a dielectric silicon cylinder ($\varepsilon_c = 18$) of radius $r_c = 158nm$ embedded in free space. Figure 2 shows the electric field amplitude in space for the two higher multipole orders (Figure 2 (a) & (b)), as predicted by Eq.(4), in addition to the total electric field for these two orders (Figure 2 (c)). This is a case where both dipole moments generate relatively strong fields. Note that the multipoles replace the cylinder, and act as point sources located at the center of the cylinder. As a visual aid, the outline of the cylinder is also drawn in the figure.

In order to test the validity of our approach, we also compare the total fields as extracted from the dipole moments (Eq. (4) and Figure 2 (c)) to the total field outside the cylinder as predicted from the rigorous Mie scattering theory [46], including all scattering orders. This result is presented in Figure 2 (d) and shows that despite some subtle differences near the cylinder surface, the fields are overall described very well by the multipole approximation treatment. This indicates that a metamaterial scatterer could be replaced by the much easier to handle multipole point sources, without sacrificing significant accuracy in the field description.

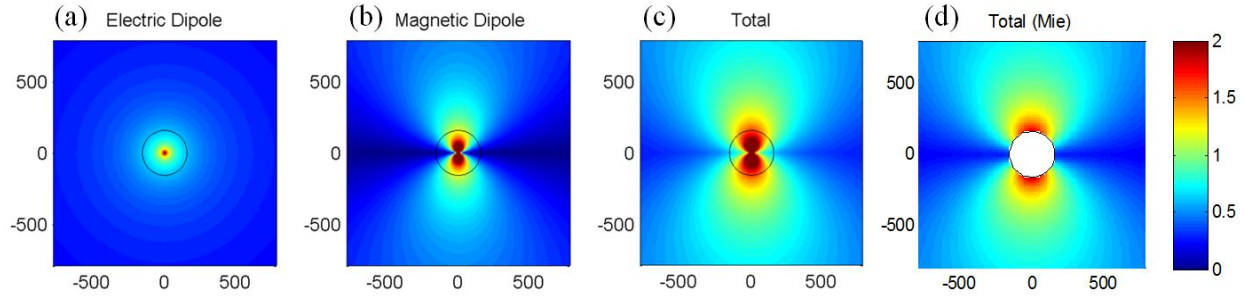

Figure 2: The excited magnetic field amplitude distribution E_z for the first two multipole orders under monochromatic plane wave excitation at 632 nm. A dielectric cylinder with $r_c = 158\,nm$ and $\varepsilon_c = 18$ embedded in free space is assumed. The multipoles act as sources, replacing the cylinder's scattered fields. As a comparison, the cylinder's perimeter is noted by the thin black line. The fields in all panels are normalized to the same value. The horizontal (x) and vertical (y) axes represent position in nm. (c): The total field produced by the multipole moments. (d): The scattered fields outside the cylinder as predicted from Mie scattering theory. Note that in (d) the fields inside the cylinder are not shown for fair comparison with the multipole treatment which only relates to scattered fields.

III. MULTIPOLE POLARIZABILITIES FOR DIELECTRIC CYLINDERS

In this section we focus on the case of a dielectric cylindrical rod illuminated by TM & TE waves, and calculate the electric, magnetic, and quadrupole polarizabilities for these structures. The polarizabilities are written as a function of the known cylindrical Mie scattering coefficients, and are also evaluated under the quasistatic and static approximations.

The cylinder is assumed to have a relative permittivity ε_c and radius r_c, while the background material is also assumed to be non-magnetic with relative permittivity ε_b. We assume perpendicularly incident plane wave monochromatic excitations of the form $\vec{E}^i_{TM} = \hat{z}\, e^{+jk_b x}\ V/m$ for TM waves and $\vec{E}^i_{TE} = +\hat{y} Z_b e^{+ik_b x}\ V/m$ for TE waves, as shown in Figure 1. These incident fields will polarize the molecules of the dielectric material, generating a polarization density $\vec{P}$. This in turn will excite longitudinal polarization currents J_z in the TM case and J_x, J_y in the TE case. In order to link the Mie coefficients with the multipole moments, we follow the approach suggested in [37] and match the far field expression retrieved using the multipole expansion (Eq. (5)) with the well-known far field expressions for scattering from a dielectric cylinder that involves the Mie coefficients,[46] which are

$$\begin{aligned} \vec{E}_{TM} &\overset{k_b r \gg 1}{\simeq} -\hat{z}\left[b_0 + 2b_1\cos\varphi + 2b_2\cos 2\varphi\right] 4jG_\infty \\ \vec{H}_{TE} &\overset{k_b r \gg 1}{\simeq} -\hat{z}\left[a_0 + 2a_1\cos\varphi + 2a_2\cos 2\varphi\right] 4jG_\infty \end{aligned} \quad . \tag{7}$$

The a and b Mie coefficients are assumed to be known, and encompass all the information of the scatterer, such as its radius r_c, its permittivity ε_c, as well as the permittivity ε_b of the background

medium. The implicit hypothesis here is that the polarizabilities that correctly predict the far fields will also correctly describe the fields anywhere else in space. Note also that (7) has an even dependence on φ, which applies to scatterers symmetric with respect to the x-axis.

We now directly compare Eqs. (5) and (7), noting that the terms m_x, p_x, Q_{xx} and Q_{yy} vanish because the symmetry of the structure and the excitation impose that the polarization current components are even functions of the space coordinate y'. The excited moments in terms of the Mie coefficients become

$$\begin{array}{lll} \vec{p}_{TM} = +\hat{z}\dfrac{4b_0}{jk_b^2 Z_b c_b} & \vec{m}_{TM} = -\hat{y}\dfrac{4b_1}{jk_b^2 Z_b} & \ddot{Q}_{TM} = \ddot{0} \\ \vec{p}_{TE} = +\hat{y}\dfrac{8a_1}{jk_b^2 c_b} & \vec{m}_{TE} = +\hat{z}\dfrac{4a_0}{jk_b^2} & \ddot{Q}_{TE} = \left(\hat{x}\hat{y}+\hat{y}\hat{x}\right)\dfrac{16a_2}{k_b^3 c_b} \end{array} . \tag{8}$$

In this 2D system the units of the electric dipole, magnetic dipole, and electric quadrupole moments are Cb, $A\cdot m$, and $Cb\cdot m$, respectively. The electric dipole polarizability $\ddot{\alpha}^e$ is then defined through the equation $\vec{p} = \varepsilon_0\varepsilon_b\ddot{\alpha}^e\cdot\vec{E}^i$, the magnetic dipole polarizability $\ddot{\alpha}^m$ through $\vec{m} = \ddot{\alpha}^m\cdot\vec{H}^i$, and the electric quadrupole polarizability $\ddot{\ddot{\alpha}}^q$ through $\ddot{Q} = \varepsilon_0\varepsilon_b\ddot{\ddot{\alpha}}^q\cdot\vec{E}^i$, with ε_0 the free space permittivity and ε_b the relative permittivity of the background medium. The nonzero elements of the dipole polarizability tensors are as follows:

$$\begin{array}{lll} \alpha_{xx}^e = \alpha_{yy}^e = \dfrac{8a_1}{jk_b^2} & \overset{k_b r_c \ll 1}{\simeq} \left(\pi r_c^2\right) 2\dfrac{\dfrac{\varepsilon_c}{\varepsilon_b}\cdot g_1\left(k_c r_c\right) - 1}{\dfrac{\varepsilon_c}{\varepsilon_b}\cdot g_1\left(k_c r_c\right) + 1} & \overset{k_c r_c \ll 1}{\simeq} \left(\pi r_c^2\right) 2\dfrac{\dfrac{\varepsilon_c}{\varepsilon_b} - 1}{\dfrac{\varepsilon_c}{\varepsilon_b} + 1} \\ \alpha_{zz}^e = \dfrac{4b_0}{jk_b^2} & \overset{k_b r_c \ll 1}{\simeq} \left(\pi r_c^2\right)\dfrac{\left(2\dfrac{\varepsilon_c}{\varepsilon_b} - 1\right) g_1\left(k_c r_c\right) - 1}{g_1\left(k_c r_c\right) + 1} & \overset{k_c r_c \ll 1}{\simeq} \left(\pi r_c^2\right)\left(\dfrac{\varepsilon_c}{\varepsilon_b} - 1\right). \\ \alpha_{xx}^m = \alpha_{yy}^m = \alpha_{zz}^m = \dfrac{4b_1}{jk_b^2} = \dfrac{4a_0}{jk_b^2} & \overset{k_b r_c \ll 1}{\simeq} \left(\pi r_c^2\right)\dfrac{g_1\left(k_c r_c\right) - 1}{g_1\left(k_c r_c\right) + 1} & \overset{k_c r_c \ll 1}{\simeq} 0 \end{array} \tag{9}$$

Here k_c is the wavevector inside the cylinder, while $g_1(x) = J_1(x)\big/ xJ_1'(x)$.

In addition to the relation between the polarizabilities and the Mie coefficients, two levels of approximation are presented in Eq. (9). The first is that the wavelength inside the background medium is much larger compared to the cylinder diameter, or $k_b r_c \ll 1$ (quasistatic limit). This condition is usually required in metamaterials in order for the incident light to perceive the structure as a continuous medium, where effective material parameters can be assigned. If, in addition to $k_b r_c \ll 1$, we also impose $k_c r_c \ll 1$ (static limit), then the wavelength inside the cylinders as well is also much larger than their radius. In that case the well-known static electric polarizabilities of dielectric cylinders are retrieved, while any magnetic

response of the cylinders disappears. The plasmonic resonance condition for cylinders, $\varepsilon_c = -\varepsilon_b$, is also retrieved for the static case of the electric polarizability.

Already at this stage it can be seen that if negative permeability is to be achieved with a dielectric metamaterial, the condition $k_c r_c \ll 1$ must not be allowed, implying that high-permittivity materials must be utilized. As an example, Figure 3 shows the electric and magnetic polarizabilities of a silicon cylinder at optical frequencies ($\varepsilon_c = 18$) embedded in free space, normalized to the cylinder's cross sectional area πr_c^2, as a function of its radius normalized to the free space wavelength λ_0, for the approximations discussed above.

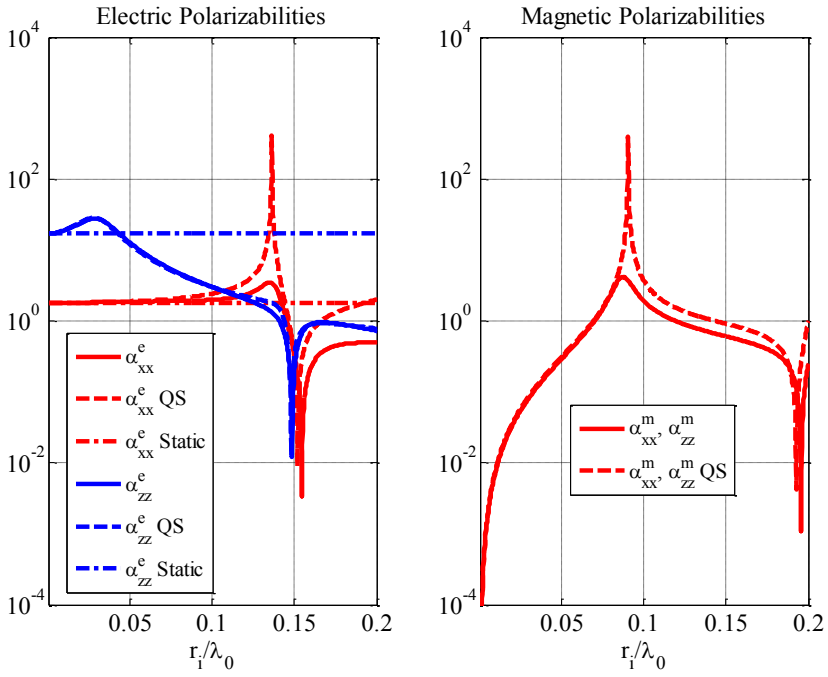

Figure 3: Longitudinal (a_{zz}) and transverse ($a_{xx} = a_{yy}$) electric (a) and magnetic (b) polarizabilities as a function of the normalized radius for a cylindrical rod made from silicon ($\varepsilon_c = 18$) embedded in free space. The polarizabilities are normalized to the rod's cross sectional area πr_c^2, and are also shown under the QS-quasistatic ($k_b r_c \ll 1$) and static ($k_c r_c \ll 1$) approximations. Note that no magnetic response occurs in the static limit. A perpendicularly incident plane wave propagating along the y-axis is assumed, as shown in Figure 1.

Figure 3 is representative of polarizability resonances, indicating their width and strength for high-ε dielectric metamaterials. It is important to note here that unless one operates in the static limit, a single incident wave will simultaneously excite both electric and magnetic resonances, generating both electric and magnetic responses from the material. This is extremely important to consider in the design of

composite media: when attempting to excite artificial magnetism, for example, some electric effects will be inevitably excited as well, unless a properly designed element is used[48]. This is why it is of great interest to be able to predict the locations of the resonances for the various material parameters, because the most unusual artificial electromagnetic properties will occur around these resonances. This is the goal of the next section.

IV. MAPING THE POLARIZABILITY RESONANCES FOR DIELECTRIC CYLINDERS

In this section we examine the locations of the electric and magnetic polarizability resonances for high-ε dielectric cylinders as a function of the cylinder's radius, its permittivity, as well as the background permittivity.

From Eq. (9), the analytical expressions that describe the conditions for a polarizability resonance can be directly derived, for each level of approximation:

$$\begin{aligned}
&\alpha_{xx}^{e},\alpha_{yy}^{e}:a_1^{-1}\to 0 && \overset{k_b r_c\ll 1}{\Rightarrow}\ g_1(k_c r_c)=-\frac{\varepsilon_b}{\varepsilon_c} && \overset{k_c r_c\ll 1}{\Rightarrow}\ \varepsilon_b=-\varepsilon_c\\
&\alpha_{zz}^{e}: \quad b_0^{-1}\to 0 && \overset{k_b r_c\ll 1}{\Rightarrow}\ g_1(k_i r_i)=\frac{1}{2\frac{\varepsilon_i}{\varepsilon_b}-1} && \overset{k_c r_c\ll 1}{\Rightarrow}\ \varnothing\\
&\alpha_{xx}^{m},\alpha_{yy}^{m},\alpha_{zz}^{m}:a_0^{-1},b_1^{-1}\to 0 && \overset{k_b r_c\ll 1}{\Rightarrow}\ g_1(k_c r_c)=-1 && \overset{k_c r_c\ll 1}{\Rightarrow}\ \varnothing
\end{aligned} \tag{10}$$

It is observed that in the static limit (rightmost formulas), as expected, only the transverse plasmonic polarizability resonance can be achieved, while in the quasistatic limit transcendental equations need to be numerically solved.

The simplest example is the case of the resonance for the magnetic polarizability α_{xx}^{m}, where the approximate equation $g_1(k_c r_c)=J_1(k_c r_c)\big/k_c r_c J_1'(k_c r_c)=-1$ predicts that the first magnetic resonance will appear at a free space wavelength $\lambda_0=2\pi r_c\sqrt{\varepsilon_c}\big/p_1$, where $p_1\simeq 2.405$ is the first zero of the Bessel function of zeroth order. As an example, for silicon ($\varepsilon_c\simeq 18$) nanorods with 50 nm radius embedded in free space, this resonance will appear around $\lambda_0\simeq 555nm$. This type of resonance has been identified experimentally for mid-infrared frequencies using a lattice of silicon carbide nanorods[35]. The same equation also indicates that increased cylinder permittivity lowers the frequency of the resonance.

The dependence of the resonances on the cylinder's relative permittivity is first examined, by numerically solving Eq. (10) for the full case (no approximations). The permittivity is varied between 5 and 30, while assuming a free space background medium. The locations of the first (lowest frequency) electric and magnetic dipole polarizability resonances as a function of the cylinder radius normalized to the free space wavelength, r_c/λ_0, are presented in Figure 4. Higher order resonances may be available as

well (as the value of r_c/λ_0 is increased), however they are usually weaker and thus only the lowest one is examined here.

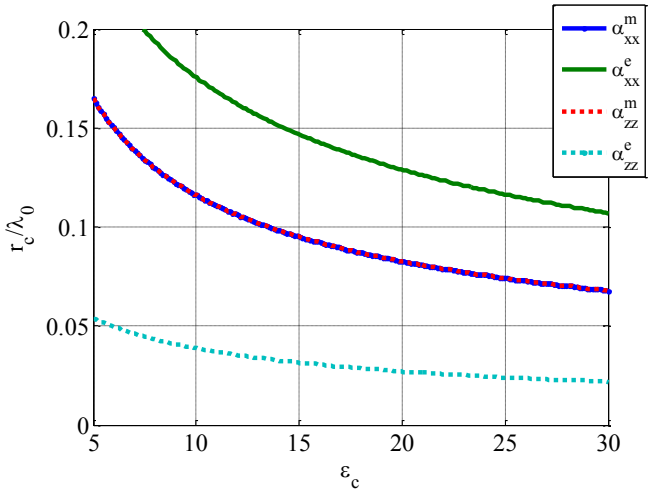

Figure 4: The locations of the electric and magnetic polarizability resonances as a function of a cylindrical rod's relative permittivity embedded in free space. The full description (a) and the quasistatic approximation (b) yield very similar results. The magnetic resonances are isotropic, occurring at the same frequency for both the longitudinal (α_{zz}^m) and transverse (a_{xx}^m) magnetic polarizabilities, while the electric resonances simultaneously occur on either side of the magnetic one.

It is observed that the locations of the polarizability resonances follow the same qualitative trends. In accordance with the analytically tractable case for the transverse magnetic polarizability α_{xx}^m that was examined earlier, the resonant frequency is shifted lower for all polarizabilities as ε_c is increased. In addition, the mathematical property that $\alpha_0 = b_1$ is reflected by the overlap of the α_{xx}^m and α_{zz}^m curves. It is also worth noting that a single field excitation (TE or TM) will always simultaneously generate both electric and magnetic types of resonances, with different strengths and at different frequencies. For a given geometry, the magnetic resonances for TE and TM waves always appear at the same frequency, while the electric resonance can be placed either above or below the magnetic one, depending on the polarization.

Next, we study the locations of the polarizability resonances as a function of the non-magnetic background medium and its relative permittivity ε_b. The shape of the excited resonance on the dielectric cylinder is highly dependent on the value of ε_b. We divide the behavior into three categories. First, there is the case where the background is a plasmonic medium ($\varepsilon_b < 0$). Second, there is the case where a high contrast ratio is maintained between the permittivity of the cylinder and that of the background

($0 < \varepsilon_b \ll \varepsilon_c$). Finally, there is the case where this contrast ratio is low. Figure 5 shows the electric and magnetic longitudinal polarizability values a_{zz}^e and a_{zz}^m normalized to the cylinder cross sectional area as a function of its normalized radius, for three different background media with $\varepsilon_b = -1$, $\varepsilon_b = 1$, and $\varepsilon_b = 3.5$. As before, the cylinder is assumed to be made of silicon with $\varepsilon_c = 18$.

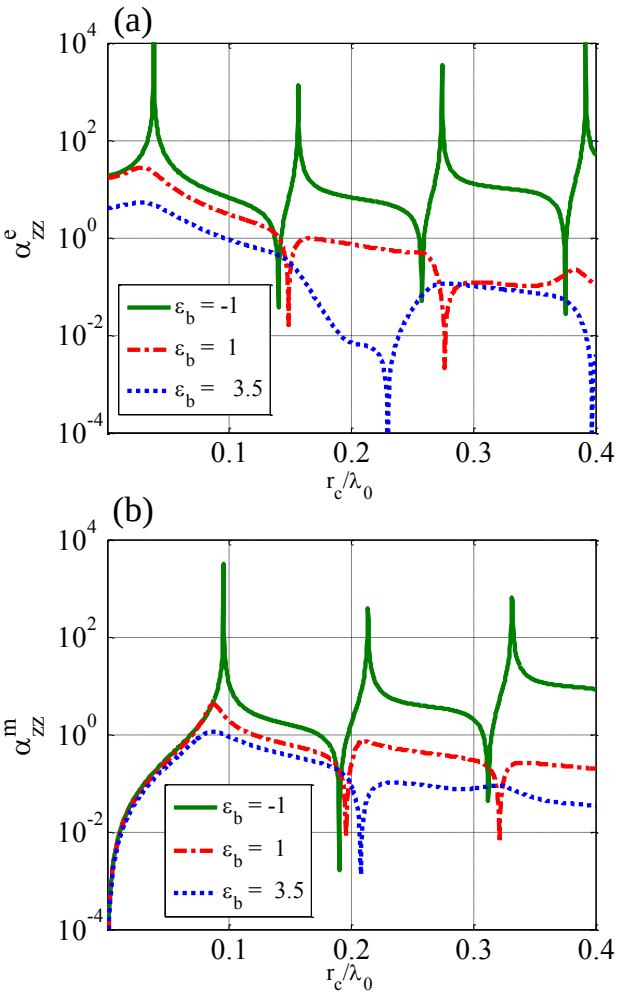

Figure 5: The electric (a) and magnetic (b) transverse polarizability responses normalized to the rod's cross sectional area as a function of the normalized radius for a silicon ($\varepsilon_c = 18$) cylinder embedded in three different background media with $\varepsilon_b = 1$ (dotted-dashed line), $\varepsilon_b = 3.5$ (dotted line) and $\varepsilon_b = -1$ (solid line), respectively. Qualitatively similar responses appear for the longitudinal polarizabilities as well.

The resonant features of the dipole polarizabilities presented in Figure 5 follow similar patterns. For cylinders embedded in free space, $\sqrt{\varepsilon_c/\varepsilon_b} \simeq 4.2$ and there exist clearly distinct resonances (dotted-dashed lines). When the index contrast is lowered to $\sqrt{\varepsilon_c/\varepsilon_b} \simeq 2.3$, the resonances broaden and weaken,

while not significantly shifting in frequency (dotted lines). When a plasmonic material is assumed as a background, the resonances become very sharp and strong for both polarizabilities. This strongly indicates the presence of a negative permeability band around these locations. This phenomenon is extremely encouraging as a strong negative permittivity and permeability response can be extracted from dielectric rods surrounded by a plasmonic medium. It should also be noted that the sharp dips that appear in the polarizability plots correspond to well-known "cloaking" schemes where minimum excitation is observed from the metamaterial [6].

To complete the picture of the dependence of the resonances on the background medium, the locations of the first (lowest frequency) electric and magnetic polarizability resonances as ε_b is varied are shown in Figure 6. It is observed that the locations of the resonances are relatively insensitive to the background medium permittivity. This is advantageous in attempting to identify the resonances experimentally, while the tuning of the frequency of interest can be achieved by controlling the size of the metamaterial unit element.

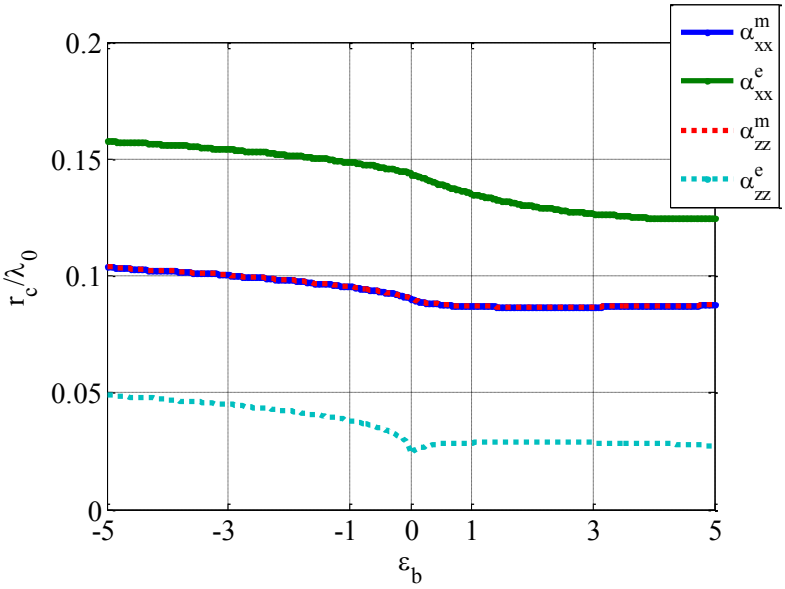

Figure 6: The locations of the lowest frequency electric and magnetic polarizability resonances for silicon cylindrical rods as a function of the relative permittivity of the background medium.

V. CONCLUSIONS

In this work we theoretically studied the resonating properties of two-dimensional optical metamaterial elements made from all-dielectric materials. The purpose of this study was to identify the behavior of the magnetic and electric polarizability resonances, since the desired unusual responses of metamaterials such as optical magnetism are expected to occur in the neighborhood of these resonances. A novel analytical framework was developed based on a two-dimensional multipole expansion that

describes the electric and magnetic fields generated via the polarization currents when a 2D element is excited by both TE and TM plane waves propagating perpendicularly to the element's axis. The polarizabilities where then derived for the case of dielectric cylinders as a function of the cylindrical Mie coefficients, and the proper approximate forms under the quasistatic and static approximations were also presented.

Finally, it should be pointed out that all-dielectric materials typically give rise simultaneously to relatively broad electric and magnetic resonances. When plasmonic materials are utilized, the resonant lineshapes are narrower and the mode interference produces non-Lorentzian Fano-type resonances[49].

This work was implemented within the framework of the Action "Supporting Postdoctoral Researchers" of the Operational Program "Education and Lifelong Learning" (Action's Beneficiary: General Secretariat for Research and Technology), and was co-financed by the European Social Fund and the Greek State. The work was also partly supported by the Archimedes Center for Modeling, Analysis and Computation (ACMAC, project FP7-REGPOT-2009-1).

VI. APPENDIX

In this Appendix we detail the analytical steps for deriving the multipole scattering formulation for a cylindrical dielectric object with infinite extent along its axis and arbitrary cross-section. We begin with Maxwell's equations satisfied by the electromagnetic field everywhere in space (including the dielectric interior)

$$\nabla \times \vec{E} = j\omega\mu_0 \vec{H}, \quad \nabla \times \vec{H} = \vec{J} - j\omega\varepsilon_0\varepsilon_b \vec{E}, \tag{A1}$$

where $\vec{J}(\vec{r}) = -j\omega\varepsilon_0 \Delta\varepsilon(\vec{r})\vec{E}(\vec{r})$ is the polarization current and $\Delta\varepsilon(\vec{r}) = \varepsilon(\vec{r}) - \varepsilon_b$ is the relative permittivity contrast of an arbitrary point in space relative to the background medium. For a homogeneous material, $\Delta\varepsilon = \varepsilon_c - \varepsilon_b$ inside the scatterer and zero outside, a discontinuity that has important implications discussed in the following. In the 2D scenario where the cylinder axis is in the z direction, the gradient operator becomes $\nabla = \hat{x}\partial/\partial x + \hat{y}\partial/\partial y$. Moreover, as a corollary of the invariance along *z*, the electromagnetic fields decouple into two independent states of polarizations, namely the transverse magnetic (TM) and transverse electric (TE), with components E_z, H_x, H_y and H_z, E_x, E_y, respectively. Each stated is excited by illuminating the cylinder with a plane EM wave with the corresponding polarization and then the total field can be expressed as the sum of the scattered and incident waves, the latter being the solution in the limit of a transparent scatterer. To obtain the multipole formulation, the field is first written in terms of the vector and scalar potentials produced by the current distribution $\vec{J}$

$$\vec{E} = j\omega\vec{A} - \nabla\varphi, \quad \vec{H} = \mu_0^{-1}\nabla\times\vec{A}, \tag{A2}$$

which, under the Lorentz assumption $\nabla\cdot\vec{A} = j\omega\varepsilon_0\mu_0\Phi$, satisfy the independently solvable wave equations

$$\left(\nabla^2 + k_0^2\right)\vec{A} = -\mu_0\vec{J}, \quad \left(\nabla^2 + k_0^2\right)\Phi = -\frac{\rho}{\varepsilon_0\varepsilon_b}, \tag{A3}$$

where $\rho = \varepsilon_0\varepsilon_b\nabla\cdot\vec{E}$ is the polarization charge density (in Cb/m^3). The latter is connected to the gradient of the polarization current through the continuity equation $\rho = \nabla\cdot\vec{J}\,/\,j\omega$. The solutions to Eqs. (A3) are readily obtained as radiation integrals

$$\begin{aligned}\vec{A}(\vec{r}) &= \mu_0\int G(\vec{r}-\vec{r}')\vec{J}(\vec{r}')dS', \\ \varphi(\vec{r}) &= \frac{1}{\varepsilon_0\varepsilon_b}\left[\int G(\vec{r}-\vec{r}')\rho(\vec{r}')dS' + \oint G(\vec{r}-\vec{r}')\sigma(\vec{r}')d\ell'\right]\end{aligned} \tag{A4}$$

where $G(\vec{r}-\vec{r}') = \frac{j}{4}H_0^{(1)}(k_b\,|\vec{r}-\vec{r}'\,|)$ is Green's function in two dimensions for a $e^{-j\omega t}$ time dependence and the dS' integration takes place over the cross-section of the dielectric rod. Attention should be paid to the second term in the expression of the scalar potential which is a line integral of the *surface* charge density (σ in Cb/m^2) over the boundary of the cylinder. The surface density arises in the case of TE polarized fields from the discontinuity of the normal component of the polarization current at the dielectric interface, and is expressed as $\sigma = -\vec{J}\cdot\hat{s}\,/\,j\omega$, where $\hat{s}$ is the outward unit normal to the interface. In case of TM fields, the current is directed along the *z* axis and is independent of *z* hence there is no accumulation of volume or surface charge ($\rho = 0, \sigma = 0$). Therefore in the TM case the scalar potential vanishes $(\Phi = 0)$ while the vector potential has a single *z* component $(\vec{A} = \hat{z}A_z)$.

The multipole expansion of the fields is obtained by Taylor-expanding Green's function with respect to the point of integration inside the scatterer

$$G(\vec{r}-\vec{r}') = G(\vec{r}) - \vec{r}'\cdot\nabla G(\vec{r}) + \frac{1}{2}(\vec{r}'\cdot\nabla)^2 G(\vec{r}) + \ldots \tag{A5}$$

Each term in this series gives rise to a particular moment. For $k_b\,|\vec{r}\,'| \ll 1$, the contribution of the higher-order terms becomes increasingly weak allowing a fair approximation of the solution with a finite number of terms. Focusing on the first three terms, the scalar potential from Eq. (A4) is approximated in the TE case as

$$\Phi_{TE} \cong \frac{q}{\varepsilon_0\varepsilon_b}G - \frac{\vec{p}}{\varepsilon_0\varepsilon_b}\cdot\nabla G + \frac{\ddot{Q}}{2\varepsilon_0\varepsilon_b}:\nabla\nabla G, \tag{A6}$$

where the dependence of φ and G on $\vec{r}$ has been omitted for brevity. Here

$$
\begin{aligned}
q &= \int \rho(\vec{r}')\,dS' + \oint \sigma(\vec{r}')\,d\ell', \\
\vec{p} &= \int \rho(\vec{r}')\,\vec{r}'\,dS' + \oint \sigma(\vec{r}')\,\vec{r}'\,d\ell', \\
\ddot{Q} &= \int \rho(\vec{r}')\,\vec{r}'\otimes\vec{r}'\,dS' + \oint \sigma(\vec{r}')\,\vec{r}'\otimes\vec{r}'\,d\ell'
\end{aligned}
\tag{A7}
$$

are the total (volume and surface) electric charge, dipole and quadrupole moments, respectively, and $\otimes$ denotes the dyadic product between two vectors. It should be kept in mind that, in 2D, the charge and moment units are normalized per unit length, i.e. q is in *Cb*/*m*, $\vec{p}$ in *Cb* and $\ddot{Q}$ in *Cb*·*m*. Note also that the operator $(\vec{r}'\cdot\nabla)^2$ in Eq. (A6) has been replaced by the dyadic double-dot product $\vec{r}'\vec{r}':\nabla\nabla$. The monopole term can be shown to be zero as expected for a neutral object. Indeed, by the divergence theorem: $j\omega q = \int \nabla'\cdot\vec{J}\,dS' - \oint \vec{J}\cdot\hat{s}\,d\ell' = 0.$ In addition, the dipole and quadrupole moments can be related to the polarization current by making use of the identities

$$
\begin{aligned}
\int (\nabla'\cdot\vec{J})\,\vec{r}'\,dS' &= \oint (\vec{J}\cdot\hat{s})\,\vec{r}'\,d\ell' - \int \vec{J}\,dS', \\
\int (\nabla'\cdot\vec{J})\,\vec{r}'\otimes\vec{r}'\,dS' &= \oint (\vec{J}\cdot\hat{s})\,\vec{r}'\otimes\vec{r}'\,d\ell' - \int (\vec{J}\otimes\vec{r}' + \vec{r}'\otimes\vec{J})\,dS'
\end{aligned}
\tag{A8}
$$

where ∇' means that the operator acts on the primed coordinates x', y'. The first of the Eqs. (A8) can be proved by integrating the identity $(\nabla'\cdot\vec{J})x' = \nabla'\cdot(\vec{J}x') - \vec{J}\cdot\hat{x}$ over the cylinder's cross-section and by applying the divergence theorem for the first term in the right-hand side (and similarly for the *y* component). The second dyadic identity is shown in a similar way for any of the components of the dyadic. For example, for the *xy* component one integrates the identity $(\nabla'\cdot\vec{J})x'y' = \nabla'\cdot(\vec{J}x'y') - [(\vec{J}\cdot\hat{x})y' + (\vec{J}\cdot\hat{y})x']$ and so on. Dividing Eqs. (A8) by $j\omega$ and recalling the continuity equations and the definitions (A7), it is straightforward to obtain the first and third of Eqs. (1), which are here repeated for convenience

$$
\vec{p} = \frac{\dot{j}}{\omega}\int \vec{J}\,dS', \quad \ddot{Q} = \frac{\dot{j}}{\omega}\int (\vec{J}\otimes\vec{r}' + \vec{r}'\otimes\vec{J})\,dS' \tag{A9}
$$

Expanding the quadrupole dyadic into its components we readily obtain the 2×2 leading principal submatrix of matrix $\ddot{Q}$ in Eq. (3). From Eqs. (A7) and (A9) it follows that the dipole and quadrupole moments of the polarization charge are equivalent to zero- and first-order order moments of the polarization current, respectively.

We now turn to Eq. (A4) and the vector potential. Using again the Taylor expansion (A5) we obtain

$$
\vec{A} \simeq \mu_0\left(\int \vec{J}(\vec{r}')\,dS'\right)G - \mu_0\left(\int \vec{J}(\vec{r}')\otimes\vec{r}'\,dS'\right)\cdot\nabla G, \tag{A10}
$$

which is valid for both TE and TM fields. Note that we have now kept only the first two terms of the Taylor series, in order to obtain the same degree of approximation with the scalar potential, i.e. up to the a first-order moment of $\vec{J}$. The first integral in the right-hand side of Eq. (A10) is readily recognized from Eq. (A9) as the electric dipole moment. For the second integral we decompose the dyadic as

$$\vec{J}\otimes\vec{r}' = \frac{1}{2}\left(\vec{J}\otimes\vec{r}' + \vec{r}'\otimes\vec{J}\right) + \frac{1}{2}\left(\vec{J}\otimes\vec{r}' - \vec{r}'\otimes\vec{J}\right) \tag{A11}$$

The first symmetric dyadic is recognized from Eq. (A9) as the quadrupole moment. The second antisymmetric dyadic can be cast into a simpler form by noting that for any vector $\vec{b}$

$$\left(\vec{J}\otimes\vec{r}' - \vec{r}'\otimes\vec{J}\right)\cdot\vec{b} = \left(\vec{r}'\cdot\vec{b}\right)\vec{J} - \left(\vec{J}\cdot\vec{b}\right)\vec{r}' = \left(\vec{r}'\times\vec{J}\right)\times\vec{b} \tag{A12}$$

Using the above Eq. (A10) is brought into its final form

$$\vec{A} \simeq -j\omega\mu_0\vec{p}G + \frac{j\omega\mu_0}{2}\ddot{Q}\cdot\nabla G - \mu_0\vec{m}\times\nabla G \tag{A13}$$

where $\vec{m} = \frac{1}{2}\int \vec{r}'\times\vec{J}dS'$ is the magnetic dipole moment associated with the polarization current. Although Eq. (A13) is a general one, it is useful to emphasize that, in the case of TM fields, the term depending on $\ddot{Q}$ does not physically represent an electric quadrupole moment because a *z*-directed and *z*-invariant current does not produce volume or surface charge densities. In fact the contribution of the "quadrupole" term is equal to that of magnetic dipole (or the quadrupole moment degenerates to magnetic dipole moment as mentioned previously) and the vector potential reduces to

$$\vec{A}_{TM} \simeq -j\omega\mu_0\vec{p}G - 2\mu_0\vec{m}\times\nabla G \tag{A14}$$

The factor 2 has also been spotted in Eqs. (5).

Substituting the approximations of the potentials from Eqs. (A6) and (A13) into Eqs. (A2) we obtain the multipole expansion of the EM fields of Eq. (2), which are generally valid for both polarizations. In the TM case however the use of the reduced expressions

$$\begin{aligned} \vec{E}_{TM} / Z_b &= k_b^2 c_b \vec{p}G - 2jk_b\nabla G\times\vec{m} \\ \vec{H}_{TM} &= -jk_b\left[\nabla G\times\vec{p}c_b\right] + 2\left[k_b^2\vec{m}G + \left(\vec{m}\cdot\nabla\right)\nabla G\right] \end{aligned} \tag{A15}$$

may be more convenient and intuitive. The polar expression of Eqs. (2) are straightforward to obtain and have been given in Eq. (4). For the sake of completeness we here quote the corresponding Cartesian forms of the transverse fields $\vec{E}_{TE}$ and $\vec{H}_{TM}$. For the magnetic fields, we have

$$\vec{H}_{TM} = \hat{x}k_b^2\left\{\left[2G+\left(G''+\frac{G'}{k_br}\right)+\left(G''-\frac{G'}{k_br}\right)\cos 2\varphi\right]m_x+\left(G''-\frac{G'}{k_br}\right)m_y\sin 2\varphi - ip_zc_bG'\sin\varphi\right\}$$
$$+\hat{y}k_b^2\left\{\left[2G+\left(G''+\frac{G'}{k_br}\right)-\left(G''-\frac{G'}{k_br}\right)\cos 2\varphi\right]m_y+\left(G''-\frac{G'}{k_br}\right)m_x\sin 2\varphi + ip_zc_bG'\cos\varphi\right\} \quad \text{(A16)}$$

where the primes denote the derivatives of $G(r)=\frac{j}{4}H_0^{(1)}(k_br)$ with respect to k_br. Finally, for the electric fields we have

$$\vec{E}_{TE}/Z_b = \hat{x}\frac{k_b^2}{2}\left\{\left[2G+G''+\frac{G'}{k_br}+\left(G''-\frac{G'}{k_br}\right)\cos 2\varphi\right]p_xc_b+\left(G''-\frac{G'}{k_br}\right)p_yc_b\sin 2\varphi+2jG'm_z\sin\varphi\right\}$$
$$+\hat{y}\frac{k_b^2}{2}\left\{\left[2G+G''+\frac{G'}{k_br}-\left(G''-\frac{G'}{k_br}\right)\cos 2\varphi\right]p_yc_b+\left(G''-\frac{G'}{k_br}\right)p_xc_b\sin 2\varphi-2jG'm_z\cos\varphi\right\}$$
$$-\hat{x}\frac{k_b^2}{8}\left\{\begin{array}{l}\omega Q_{xx}\left[\left(3G'''+\frac{3G''}{k_br}+4G'-\frac{3G'}{k_b^2r^2}\right)\cos\varphi+\left(G'''-\frac{3G''}{k_br}+\frac{3G'}{k_b^2r^2}\right)\cos 3\varphi\right]+\\ \omega Q_{yy}\left[\left(G'''+\frac{G''}{k_br}-\frac{G'}{k_b^2r^2}\right)\cos\varphi-\left(G'''-\frac{3G''}{k_br}+\frac{3G'}{k_b^2r^2}\right)\cos 3\varphi\right]+\\ 2\omega Q_{xy}\left[\left(G'''+\frac{G''}{k_br}+2G'-\frac{G'}{k_b^2r^2}\right)\sin\varphi+\left(G'''-\frac{3G''}{k_br}+\frac{3G'}{k_b^2r^2}\right)\sin 3\varphi\right]\end{array}\right\}$$

$$-\hat{y}\frac{k_b^2}{8}\left\{\begin{array}{l}\omega Q_{yy}\left[\left(3G'''+\frac{3G''}{k_br}+4G'-\frac{3G'}{k_b^2r^2}\right)\sin\varphi-\left(G'''-\frac{3G''}{k_br}+\frac{3G'}{k_b^2r^2}\right)\sin 3\varphi\right]+\\ \omega Q_{xx}\left[\left(G'''+\frac{G''}{k_br}-\frac{G'}{k_b^2r^2}\right)\sin\varphi+\left(G'''-\frac{3G''}{k_br}+\frac{3G'}{k_b^2r^2}\right)\sin 3\varphi\right]+\\ 2\omega Q_{xy}\left[\left(G'''+\frac{G''}{k_br}+2G'-\frac{G'}{k_b^2r^2}\right)\cos\varphi-\left(G'''-\frac{3G''}{k_br}+\frac{3G'}{k_b^2r^2}\right)\cos 3\varphi\right]\end{array}\right\}$$

References

1 N. I. Zheludev, Science **328**, 582 (2010).
2 W. Cai and V. Shalaev, *Optical Metamaterials: Fundamentals and Applications* (Springer, 2009).
3 X. Zhang and Z. Liu, Nat Mater **7**, 435 (2008).
4 T. Ergin, J. Fischer, and M. Wegener, Physical Review Letters **107**, 173901 (2011).
5 X. Chen, Y. Luo, J. Zhang, K. Jiang, J. B. Pendry, and S. Zhang, Nat Commun **2**, 176 (2011).
6 D. Rainwater, A. Kerkhoff, K. Melin, J. C. Soric, G. Moreno, and A. Alù, New Journal of Physics **14**, 013054 (2012).
7 J. N. Anker, W. P. Hall, O. Lyandres, N. C. Shah, J. Zhao, and R. P. Van Duyne, Nat Mater **7**, 442 (2008).

[8] H. A. Atwater and A. Polman, Nat Mater **9**, 205 (2010).
[9] M. A. Green and S. Pillai, Nat Photon **6**, 130 (2012).
[10] J. A. Schuller, E. S. Barnard, W. Cai, Y. C. Jun, J. S. White, and M. L. Brongersma, Nat Mater **9**, 193 (2010).
[11] E. Ozbay, Science **311**, 189 (2006).
[12] R. Merlin, Proceedings of the National Academy of Sciences **106**, 1693 (2009).
[13] J. Zhou, T. Koschny, M. Kafesaki, E. N. Economou, J. B. Pendry, and C. M. Soukoulis, Physical Review Letters **95**, 223902 (2005).
[14] C. M. Soukoulis, T. Koschny, J. Zhou, M. Kafesaki, and E. N. Economou, physica status solidi (b) **244**, 1181 (2007).
[15] T. Ueda and T. Itoh, IEICE Electronics Express **9**, 65 (2012).
[16] Q. Zhao, J. Zhou, F. Zhang, and D. Lippens, Materials Today **12**, 60 (2009).
[17] A. E. Krasnok, A. E. Miroshnichenko, P. A. Belov, and Y. S. Kivshar, Opt. Express **20**, 20599 (2012).
[18] L. Peng, L. Ran, H. Chen, H. Zhang, J. A. Kong, and T. M. Grzegorczyk, Physical Review Letters **98**, 157403 (2007).
[19] Q. Zhao, L. Kang, B. Du, H. Zhao, Q. Xie, X. Huang, B. Li, J. Zhou, and L. Li, Physical Review Letters **101**, 027402 (2008).
[20] J. Wang, Z. Xu, B. Du, S. Xia, J. Wang, H. Ma, and S. Qu, Journal of Applied Physics **111**, 044903 (2012).
[21] J. Wang, Z. Xu, Z. Yu, X. Wei, Y. Yang, J. Wang, and S. Qu, Journal of Applied Physics **109**, 084918 (2011).
[22] J. C. Ginn, et al., Physical Review Letters **108**, 097402 (2012).
[23] N. Limberopoulos, A. Akyurtlu, K. Higginson, A.-G. Kussow, and C. D. Merritt, Applied Physics Letters **95**, 023306 (2009).
[24] V. Yannopapas and A. Moroz, Journal of Physics: Condensed Matter **17**, 3717 (2005).
[25] A.-G. Kussow, A. Akyurtlu, and N. Angkawisittpan, physica status solidi (b) **245**, 992 (2008).
[26] C. R. Simovski and S. A. Tretyakov, Physical Review B **79**, 045111 (2009).
[27] B.-J. Seo, T. Ueda, T. Itoh, and H. Fetterman, Applied Physics Letters **88**, 161122 (2006).
[28] A.-G. Kussow, A. Akyurtlu, A. Semichaevsky, and N. Angkawisittpan, Physical Review B **76**, 195123 (2007).
[29] V. Yannopapas, Applied Physics A: Materials Science & Processing **87**, 259 (2007).
[30] H. Chen, C. T. Chan, and P. Sheng, Nat Mater **9**, 387 (2010).
[31] S. O'Brien and J. B. Pendry, Journal of Physics: Condensed Matter **14**, 4035 (2002).
[32] R.-L. Chern and Y.-T. Chen, Physical Review B **80**, 075118 (2009).
[33] L. Peng, L. Ran, and N. A. Mortensen, Applied Physics Letters **96**, 241108 (2010).
[34] S. Liu, W. Chen, J. Du, Z. Lin, S. T. Chui, and C. T. Chan, Physical Review Letters **101**, 157407 (2008).
[35] J. A. Schuller, R. Zia, T. Taubner, and M. L. Brongersma, Physical Review Letters **99**, 107401 (2007).
[36] L. Kang and D. Lippens, Physical Review B **83**, 195125 (2011).
[37] K. Vynck, D. Felbacq, E. Centeno, A. I. Căbuz, D. Cassagne, and B. Guizal, Physical Review Letters **102**, 133901 (2009).
[38] A. B. Evlyukhin, S. M. Novikov, U. Zywietz, R. L. Eriksen, C. Reinhardt, S. I. Bozhevolnyi, and B. N. Chichkov, Nano Letters **12**, 3749 (2012).
[39] A. Reyes-Coronado, et al., Opt. Express **20**, 14663 (2012).
[40] S. Zouhdi, A. Sihvola, and A. P. Vinogradov, *Metamaterials and Plasmonics: Fundamentals, Modelling, Applications* (Springer, 2008).
[41] M. G. Silveirinha, Physical Review E **73**, 046612 (2006).
[42] A. B. Evlyukhin, C. Reinhardt, A. Seidel, B. S. Luk'yanchuk, and B. N. Chichkov, Physical Review B **82**, 045404 (2010).

[43] J. D. Jackson, *Classical Electrodynamics* (John Wiley & Sons, 1998).
[44] A. B. Evlyukhin, C. Reinhardt, and B. N. Chichkov, Physical Review B **84**, 235429 (2011).
[45] C. H. Papas, *Theory of electromagnetic wave propagation* (McGraw-Hill, 1965).
[46] C. F. Bohren and D. R. Huffman, *Absorption and Scattering of Light by Small Particles* (Wiley, 2008).
[47] W. T. Doyle, Physical Review B **39**, 9852 (1989).
[48] P. Grahn, A. Shevchenko, and M. Kaivola, Physical Review B **86**, 035419 (2012).
[49] B. Luk'yanchuk, N. I. Zheludev, S. A. Maier, N. J. Halas, P. Nordlander, H. Giessen, and C. T. Chong, Nat Mater **9**, 707 (2010).